Accepted Manuscript

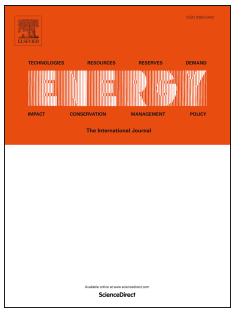

Assessing climate sensitivity of peak electricity load for resilient power systems planning and operation: A study applied to the Texas region

Panteha Alipour, Sayanti Mukherjee, Roshanak Nateghi

PII: S0360-5442(19)31413-6

DOI: https://doi.org/10.1016/j.energy.2019.07.074

Reference: EGY 15744

To appear in: *Energy*

Received Date: 22 November 2018

Revised Date: 9 July 2019

Accepted Date: 11 July 2019

Please cite this article as: Alipour P, Mukherjee S, Nateghi R, Assessing climate sensitivity of peak electricity load for resilient power systems planning and operation: A study applied to the Texas region, *Energy* (2019), doi: https://doi.org/10.1016/j.energy.2019.07.074.

Assessing climate sensitivity of peak electricity load for resilient power systems planning and operation: A study applied to the Texas region

Alipour, Pantheha[a], Mukherjee, Sayanti[b1] , Nateghi, Roshanak[c,d]

[a]*School of Engineering Technology, Purdue University, West Lafayette, IN 47907, USA*

[b]*Department of Industrial and Systems Engineering, University at Buffalo (SUNY), Buffalo, NY 14260, USA*

[c]*School of Industrial Engineering, Purdue University, West Lafayette, IN 47907, USA*
[d]*Environmental and Ecological Engineering, Purdue University, West Lafayette, IN 47907, USA*

[1] Corresponding author: Department of Industrial and Systems Engineering, The State University of New York at Buffalo, Buffalo, NY 14260, USA; Tel: +1-716-645-4699, Email address: sayantim@buffalo.edu

Highlights

- Maximum temperature is the most important predictor of climate-sensitive peak load
- Dew point temperature significantly influences peak load both during summer and winter
- Maximum sustained wind speed lowers daily peak load
- Electricity price has a strong positive association with peak load
- Economic growth of the state is inversely associated with peak load

Assessing climate sensitivity of peak electricity load for resilient power systems planning and operation: A study applied to the Texas region

Abstract

Accurate forecasting of peak electricity load has long been an active area of research in electricity markets, and power systems planning and operation. Unanticipated climate-induced surges in peak load can lead to supply shortages causing frequent brownouts and blackouts, and large-scale socioeconomic impacts. In this paper, the climate sensitivity of daily peak load is characterized by leveraging advanced statistical machine learning algorithms. More specifically, a rigorously tested and validated predictive model based on the Bayesian additive regression trees algorithm is proposed. Results from this study revealed that maximum daily temperature followed by mean dew point temperature are the most important predictors of the climate-sensitive portion of daily peak load. Among the non-climatic predictors, electricity price was found to have a strong positive association with the daily peak load. Economic growth was observed to have an inverse association with the daily peak load. While the proposed framework is established for the state of Texas, one of the most energy-intensive states with geographic and demographic susceptibility to climatic change, the methodology can be extended to other states/regions. The model can also be used to make short-term predictions of the climate-sensitive portion of daily peak load.

Keywords: Predictive energy analytics, climate sensitive peak-load, dew point

temperature, statistical learning theory

1. Introduction

Ensuring the resilience of the grid, considering a multi-dimensional perspective [1], is of utmost importance to minimize the socio-economic impacts in face of extreme events [2]. Accurate estimates of peak electricity load is an integral component of electric power system adequacy planning, contributing to its resilience [3]. Unlike many other commodities, electricity cannot be stored. Thus, supply and demand have to be matched in real-time to ensure that power is available to the consumers when the switch is turned on [4]. Adequate generation capacity and demand-side resources have to be specifically planned and built, not only to meet the maximum load and minimize blackout risks [5], but also for efficient policy planning and implementation [6]. Accurate forecasts of daily peak load can help electric utilities and energy professionals make optimal resource allocation decisions, assess the security of power systems, and adequately schedule maintenance plans. Over- or under-estimation of daily peak load will result in either excess or inadequate supply respectively, resulting in inefficient investments and expenditure patterns. The evolution of daily peak load is not deterministic and depends on many uncertain, stochastic factors [7]— including climate variability, socioeconomic condition, technology change, and population growth as well as infrastructure and building types [8].

In this paper, a generalized, probabilistic predictive framework is proposed, using a state-of-the-art Bayesian ensemble-of-trees algorithm. The proposed framework is used to characterize the sensitivity of daily peak load to climate, as climate variability and change has been projected to have significant impacts

on the evolution of peak electricity load [9]. While the proposed data-centric framework can be applied to any geographical area (contingent on data availability), geographical scope of the proposed analysis is focused on a single state. The rationale for limiting the spatial scope of this analysis is that the consumption patterns of electricity consumers are generally a function of where and how they live [10], and is influenced by regional differences in climate, infrastructure systems, policies, and societal norms [11].

The state of Texas is selected as a case study due to a number of reasons such as the state's infrastructure vulnerability to climate and weather [12]. The climate variance in Texas is attributed to its unique location and is considered to be the consequence of interactions between several weather and climate factors such as the movement of seasonal air masses (e.g., Arctic fronts) from Canada, subtropical west-winds from the Pacific Ocean and Northern Mexico, tropical cyclones or hurricanes from the Gulf of Mexico, a high pressure system in the Atlantic Ocean (aka the Bermuda High) and the movement of jet streams [13].

According to the U.S. Energy Information Administration (EIA), Texas produces more electricity than any other state, generating almost twice as much as Florida which is the second highest electricity-producing state [14]. More than three-quarter of the state's electricity is generated by independent power producers and industrial generators [14]. It is noteworthy that not only is Texas the largest electricity generating state in the country, but also one of the largest electricity consuming states, and has experienced rapid growths in both electricity demand and generation in recent years [14]. Texas experienced a notable population increase of around four million people, making the state rank among the top five largest growing states in the U.S. [14]. With rapid population growth in

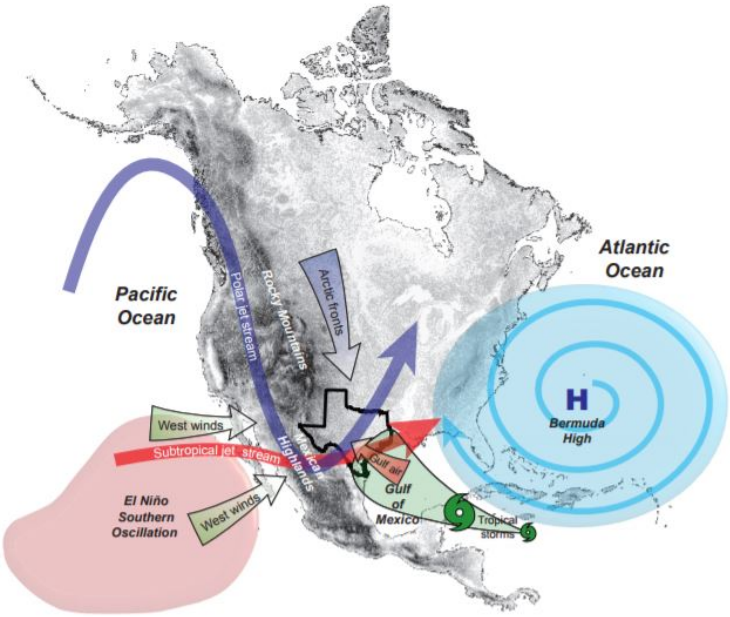

Figure 1: A schematic of the weather and climate systems in the state of Texas [13].

Dallas, Houston, Austin and San Antonio metropolitan areas, the state of Texas has led the nation in terms of annual population growth since 2006 [14].

The largest share of retail electricity sales in Texas belongs to the residential sector [14], which is most sensitive to climate variability and change [15]. A significant fraction of the households in the state use electricity as their primary heating fuel in the winter [14]. The demand for air conditioning is also substantially higher during the hot summer months. In recent years, Texas has observed multiple episodes of unexpected demand surge during periods of heatwaves. The Electric Reliability Council of Texas (ERCOT) region broke all previous records of peak demand during the 2016 hot summer months across the state [14]. Texas, therefore, exhibits a very interesting case study for understanding the nexus between climate variability and peak electricity load to inform adequate investment decisions related to electric infrastructure capacity expansions and/or reliable

power systems planning and operation .

The proposed data-centric predictive framework goes beyond the existing deterministic models with linear architecture, and uses the state-of-the-art statistical learning techniques to probabilistically assess the climate sensitivity of daily peak load in the state of Texas. The models' performance is evaluated based on both goodness-of-fit and out-of-sample predictive accuracy to ensure high generalization performance as well as its ability to explain the variance in the historical data. Then, the 'best model', selected based on both the generalizablity and goodness-of-fit principles, was used to characterize the climate-sensitivity of daily peak load in Texas.

The structure of this paper is as follows. In Section 2, a brief overview of the existing literature is presented, highlighting the current knowledge gaps. The data used in the analyses is discussed in Section 3. Sections 4 and 5 outline the methodologies and results. Section 6 concludes the paper by summarizing the key findings and delineating the future research directions.

2. Literature Review

There exists a significant body of literature in power system load forecasting. The bulk of the existing research in this area has primarily focused on short-term load forecasting (STLF). The goal of STLF is to predict the future hourly and daily loads for a service area of interest, and plays a key role in various electricity system operations planning such as identifying optimum spinning reserve capacity as well as conducting reliability analysis and security assessment.

STLF has been modeled using a wide range of approaches including (a) simulation; (b) time series models; (c) regression analysis and statistical machine

learning; and (d) and hybrid models. Below is a brief outline of the current state of knowledge in short-term load forecasting. The review starts with highlighting studies based on simpler generalized linear regression and time-series models and then progresses to more complex approaches based hybrid modeling techniques as well as machine learning techniques.

Haida and Muto [16] presented a regression-based daily peak load forecasting method consisting of a regression model to predict the nominal load, and a learning method to predict the residual load. Haida et al. [17] expanded this model by introducing two trend processing techniques designed to reduce errors in transitional seasons. Ramanathan et al. [18] leveraged multivariate regression modeling using historical data for the Puget Sound Power and Light Company. In this research, the statistical models were trained using the hourly load and weather observations during the fall and winter months of 1983–1990, in order to estimate short-term peak load. More specifically, a number of multiple linear regression (MLR) models were developed for each hour of the day. The lead-time for the forecast models ranged from 16-40 hours into the future.

Alfares and Nazeeruddin [19] presented a regression-based daily peak load forecasting method for a whole year, including holidays. To forecast load precisely throughout a year, various seasonal factors were considered. In the winter season, average wind chill factor was also added as an explanatory variable. In the transitional seasons (e.g., spring and fall), a transformation technique was used; and for holidays, a holiday effect load was deducted from the normal load.

Papalexopoulos et al. [20] developed a hybrid regression-based approach to improve the short-term system load forecasting for the Pacific Gas and Electric Company in California. The initial model consisted of an autoregressive inte-

grated moving average (ARIMA) peak load model and a MLR peak load model, which used historical data from last 15 days in the inland valley and mountain regions. The results from these two models were combined using a weighted average scheme in the initial model. The improved model removed the ARIMA peak forecast model and only relied on the MLR model. Amjady [21] proposed a time series model for short-term hourly forecasting of peak load. The results revealed that the proposed ARIMA model provided a better fit to the actual hourly peak load compared to the artificial neural network (ANN) models. Auffhammer et al. [9] used a time-series model to parameterize the relationship between peak electricity load and temperature, and estimated temperature response functions for daily peak load and total daily energy consumption for the entire U.S. They found peak load, at both the daily and annual levels, to be more sensitive to climate change than the total daily consumption. Their results showed that the impacts of climate variability on peak load varied substantially across geographical space, driven by differences in the distribution of heating and cooling degree days as well as differences in heating and cooling technologies.

Fan et al. [22] used a MLR methodology along with eight other models—including ARIMA, support vector regression (SVR), random forests (RF), multilayer perceptron (MLP), boosting tree (BT), multivariate adaptive regression splines (MARS), and k-nearest neighbors (kNN)—for predicting the next-day commercial energy consumption and peak electricity loads for the tallest buildings in Hong Kong. The authors concluded that SVR and RF models outperformed traditional statistical models such as MLR and ARIMA models. The analysis identified the peak power demand and daily energy consumption of seven days and fourteen days before the prediction day as the top four most important inputs

for the predictive models based on the random forest algorithm.

Sigauke and Chikobvu [23] developed a predictive model for daily peak demand in South Africa, using the multivariate adaptive regression splines (MARS) methodology. They demonstrated the model's capability of yielding a significantly lower root mean square error (RMSE) when compared to piecewise regression-based models. Liu et al. [24] developed a semi-parametric, two-component modeling procedure for forecasting hourly load in the eastern United States. The developed model consisted of a nonparametric component and a parametric ARIMA component. The model estimation was carried out using a modified back-fitting algorithm and was found to have a high predictive performance.

Lusis et al. [25] assessed the effects of calendar dates and forecast granularity (length of each forecast interval) on the accuracy of day-ahead household load forecast using various statistical learning techniques. Their statistical analysis demonstrated that the model based on regression trees yielded a better overall ability to predict the household load for the next 24 hours.

Chen et al. [26] applied a hybrid SVR model, both with and without multi-resolution wavelet decomposition (MWD) pre-processing, to predict hourly electric power load in a hotel building. With 15-dimensional parameters of 29 clustered days as the training sample, a nonlinear SVR model was developed. Al-Musaylh et al. [27] evaluated the performance of data-driven models based on MARS, SVR and ARIMA algorithms, for predicting short-term electricity demand using Queensland area's aggregated demand data from the Australian Energy Market Operator. For identifying significant inputs for the three prediction horizons (0.5h, 1.0h, and 24.0h), they changed the electricity demand data by applying partial autocorrelation functions. They found that the model based on the

MARS algorithm yielded the most accurate results for 0.5h and 1.0h forecasts, whereas the SVR model was better for a 24.0h horizon.

Beccali [28] used Elman's recurrent ANN algorithm to predict (with a one hour lead time) the intensity of the electric power supplied to households in a suburban area of Palermo (Italy) between June 1, 2002 and September 10, 2003. The forecasting performance of the model was tested by comparing the model predictions with the electric current intensity recorded during a summer week. The research pointed out the importance of a thermal discomfort index for a simple but effective evaluation of the conditions affecting the occupant behavior, and thus influencing the household electricity consumption related to the use of heating, ventilation and air conditioning (HVAC) appliances.

Saini and Soni [29] predicted daily peak load using a feed forward neural network (FFNN) based upon the conjugate gradient (CG) back propagation methods. They incorporated the effects of previous day peak load information, the type of day, and eleven weather parameters. The training dataset was selected using a growing window concept. To reduce the redundancies in the input space, principal component analysis (PCA) was leveraged. The resulting dataset was used to train a 3-layered neural network (NN). By comparing four different techniques, they concluded one-step secant back propagation algorithm (OSS-BP) to be the best learning technique for peak load forecasting.

Mukherjee and Nateghi [10] investigated the predictive performance of several different parametric and non-parametric statistical learning methods—e.g., generalized linear model (GLM), generalized additive model (GAM), multivariate adaptive regression splines (MARS), random forest (RF) and Bayesian additive regression trees (BART)—to investigate the nexus between total electricity con-

sumption and climate variability. They found that the model based on the BART algorithm outperformed all the other statistical learning methods.

Despite the significant recent advances in the field, as outlined above, some knowledge gaps remain. More specifically, many of the existing models focus primarily on forecasting the load (with various lead times), and do not necessarily focus on characterizing the climate-demand nexus, which is the focus of this study. In addition, the models that focus on capturing the sensitivity of daily peak load to climate variability either (a) are based on 'rigid' modeling assumptions (e.g., based on multiple linear regression and/or time series modeling); which while interpretable, tend to underperform in terms of predictive accuracy [30], or (b) focus primarily on developing accurate predictive models with very little emphasis on model inferencing and interpretation. This paper aims to bridge these gaps by proposing a generalized, probabilistic predictive framework—grounded in statistical learning theory to (a) develop an accurate predictive model, based on *both* in-sample-fit and out-of-sample predictive accuracy, (b) identify the key predictors of the climate-sensitive portion of daily peak demand, and (c) characterize and interpret the relationship between the key climate predictors and the daily peak load. While the state of Texas is selected as a case study to demonstrate the applicability of the proposed framework, the methodologies presented in this paper are generalizable to other regions.

3. Data source, description, and visualization

This section summarizes the data used to train, test and validate our daily peak load prediction models. The explanatory variables are discussed in Section 3.1, the response variable is summarized in Section 3.2, and the full data-set is

presented in Section 3.3.

3.1. Input data (explanatory variables) preparation

The two categories of explanatory variables, namely, the weather time-series, and the socio-economic data are used as input variables in this analysis. The datasets are described in the following subsections.

3.1.1. Weather data

Daily weather data was obtained from the National Climatic Data Center (NCDC) ranging from 01-January-2002 to 31-December-2017 from multiple weather stations across the geographical area of Texas. The various weather variables (see Table 1) include: daily mean temperature (TEMP), mean dew point temperature for the day (DEWP), daily mean sea level pressure (SLP), mean visibility for the day (VISB), daily mean wind speed for the day (WDSP), maximum daily sustained wind speed (MXSPD), maximum daily temperature (TMAX), minimum daily temperature (TMIN), and daily total precipitation (PRCP).

Table 1: Weather variables description

Field	Description	Unit
TEMP	Mean temperature for the day	Fahrenheit
DEWP	Mean dew point temperature for the day	Fahrenheit
SLP	Mean sea level pressure for the day	Millibars to tenths
VISB	Mean visibility for the day	Miles to tenths
WDSP	Mean wind speed for the day	knots to tenths
MXSPD	Maximum sustained wind speed of the day	knots to tenths
TMAX	Maximum daily temperature	Fahrenheit
TMIN	Minimum daily temperature	Fahrenheit
PRCP	Total daily precipitation	Inches

3.1.2. Socio-economic data

Socio-economic data was obtained from the U.S. Bureau of Labor Statistics (BLS) [31]. The data include variables such as per capita real gross state product (GSP) and unemployment percentage for the state of Texas as observed in a particular year. Monthly electricity price for the state of Texas was obtained from the U.S. Energy Information Administration (form EIA-826). The socio-economic variables are added to the analysis to serve as control variables in the models. Such non-climatic variables control for the socio-economic changes in the state of Texas over the period of analysis (2002-2017), and thus help to isolate the climate-induced effects on the electricity demand [10].

3.2. Response variable preprocessing

Hourly load data for the state of Texas was obtained from the "Hourly Load Data Archives" reported by the Electric Reliability Council of Texas (ERCOT) [32]. Also, the daily electricity sales data was extracted for the state of Texas from the U.S. Energy Information Administration (EIA) database [14]. To obtain the daily peak load data, maximum of the hourly loads recorded in a day, over the period of 01 January 2002—31 December 2017 was estimated. Similar to previous studies [33], the estimated daily peak load time-series data was detrended. Detrending was performed to remove the effect of population increase and technological growth over the years, and thus isolating the influence of climate factors on the daily peak electricity load. In order to detrend the response variable, the yearly average of the daily peak load $\overline{P}(y)$ was first calculated for the entire period of study in the following way [33]:

$$\overline{P} = \sum_{y=2002}^{2017} \sum_{d=1}^{365} E(d, y) \tag{1}$$

The adjustment factor F_{adj} for each year was calculated from:

$$F_{adj} = \overline{P}(y)^{-1} \sum_{d=1}^{365} E(d, y) \tag{2}$$

Daily peak load data was adjusted by dividing it by the adjustment factor for that year, i.e.,

$$E_{adj}(d, y) = \frac{E(d, y)}{F_{adj}} \tag{3}$$

In all the equations above, y denotes the variable "year" and d denotes the variable "day". The final analysis and model development were conducted with the trend-adjusted daily peak load data.

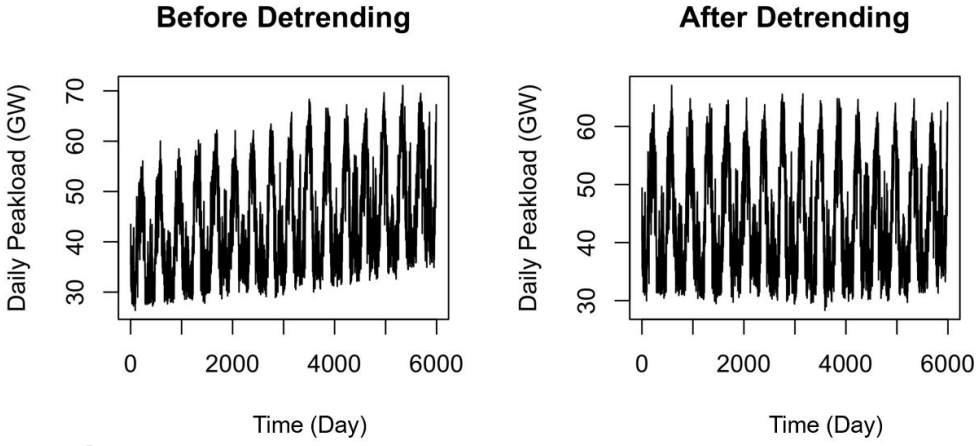

Figure 2: Daily peak electricity load (a) before detrending (left), (b) after detrending (right).

Figures 2 (a) and (b) show the raw and detrended daily peak loads, respectively. It is evident that the slight upward linear trend in Figure 2 (a) is removed after applying the de-trending methodology (Figure 2 (b)). The trend-adjusted

daily peak load time-series varies seasonally over the months, signaling climate sensitivity of the daily peak electricity load (Figure 3).

Figure 3 shows the violin plot of daily peak electricity load across the months. A violin plot combines a box-plot and a kernel density plot in one graph. More specifically, in a violin plot, a rotated kernel density plot is overlain on the two sides of a box-plot. Figure 3 shows that there is significant seasonal variations in peak electricity load. It is observed that in TX, the daily peak load is much higher during the summer months, which is expected since the use of air-conditioning is highest during the hottest days of summer, and lowest during the temperate winter months and intermediate seasons (i.e., fall and spring).

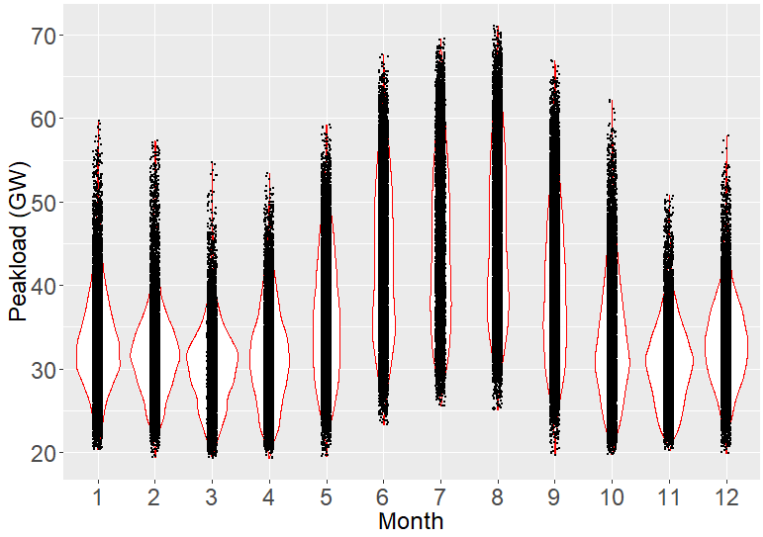

Figure 3: Violin-plot of response variable for different months.

3.3. Final data-set

The final dataset was created by combining the daily peak electricity load, weather variables, and socio-economic information, as described in Sections 3.1 and 3.2 above. Also, the days of the week is included as a control variable since

there are important differences in electricity load patterns between weekdays and weekends. The load on different weekdays can also be quite different. For example, Mondays and Fridays (adjacent to weekends) may have structurally different loads than Tuesday through Thursday. This is particularly true during the summer season. The summary statistics of the response data is presented in Table 2.

Table 2: Descriptive statistics of daily peak load (GW) during 01/01/2002–12/31/2017.

Mean	Median	Std. Dev.	Kurtosis	Skewness	Min.	Max.
36.26	34.27	9.02	0.44	0.89	19.27	71.09

Figure 4 depicts the correlation among all the selected predictors as well as the trend-adjusted response variable. In this figure, each of the variables included in the analysis is shown on the diagonal. At the bottom of the diagonal, the bivariate scatter plots with a fitted line, and at the top of the diagonal, the value of the correlation with the associated significance levels (as stars) are displayed. The significance level is denoted by stars, representing p-values of 0.001 (***), 0.01 (**), and 0.05 (*). The size of the numbers in the top diagonal represent the degree of correlation, with larger numbers (and sizes) indicating higher correlation levels and smaller numbers (and sizes) representing lower correlation levels. Figure 4 reveals that the relationship between most of the predictors and the daily peak load (response variable) is not linear. Thus, analyzing the sensitivity

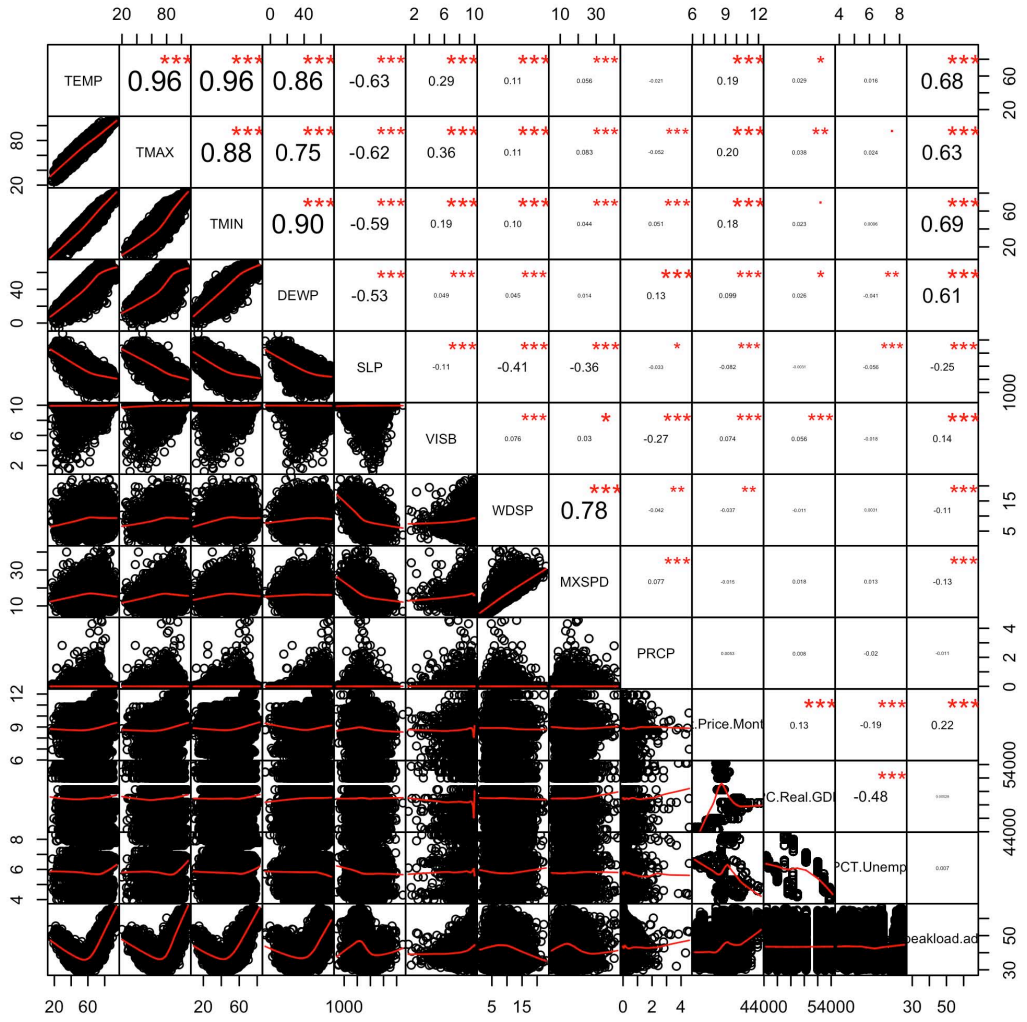

Figure 4: Correlation matrix plot.

of daily peak load using linear regression models will likely miss the potentially statistically significant non-linear relationships. Significant linear correlations are observed between the WDSP (mean wind speed) and MXSPD (maximum sustained wind speed)—with a Pearson correlation of 0.78—and between the PC.Real.GDP (per capita gross domestic product) and the PCT.Unemployment

(percentage of unemployment)—with a Pearson correlation of -0.48. Moreover, the temperature variables DEWP, TMAX, TEMP and TMIN are highly correlated with one another (Pearson correlation coefficient: $\rho > 0.8$). Therefore, to reduce masking effects due to correlation, three separate models are developed: a model with DEWP and TMAX, a second model using TMIN, a third model using TEMP, keeping all the other predictor variables same in all the models (details described in Section 5).

4. Methodology

This section presents the generalized research framework proposed in this study, and provides a brief theoretical background of the models developed to evaluate the climate sensitivity of the daily peak load for the state of Texas.

4.1. Research framework

In this research, a generalized, probabilistic predictive framework is leveraged to evaluate the climate sensitivity of the daily peak load. Figure 5 describes the various steps and flow of the proposed research. As discussed before, data on hourly electricity demand (from which the daily peak load was calculated) was collected for the state of Texas, together with various climate and weather variables as well as socio-economic information. Several types of data transformation techniques were implemented including (i) trend-adjustment of the peak load data, (ii) spatiotemporal aggregation for the climate and weather data, and (iii) inflation-adjustment on the socio-economic data, as needed. The datasets were then aggregated from various sources using year, month, and day as the key variables to generate the "Final Dataset". This step was followed by the model

development phase which is described in the subsequent subsections. As evident from this framework, while data specific to the state of Texas was used to demonstrate the applicability of the proposed research, the approach and methodology is transferable and can be extended to other geographical regions.

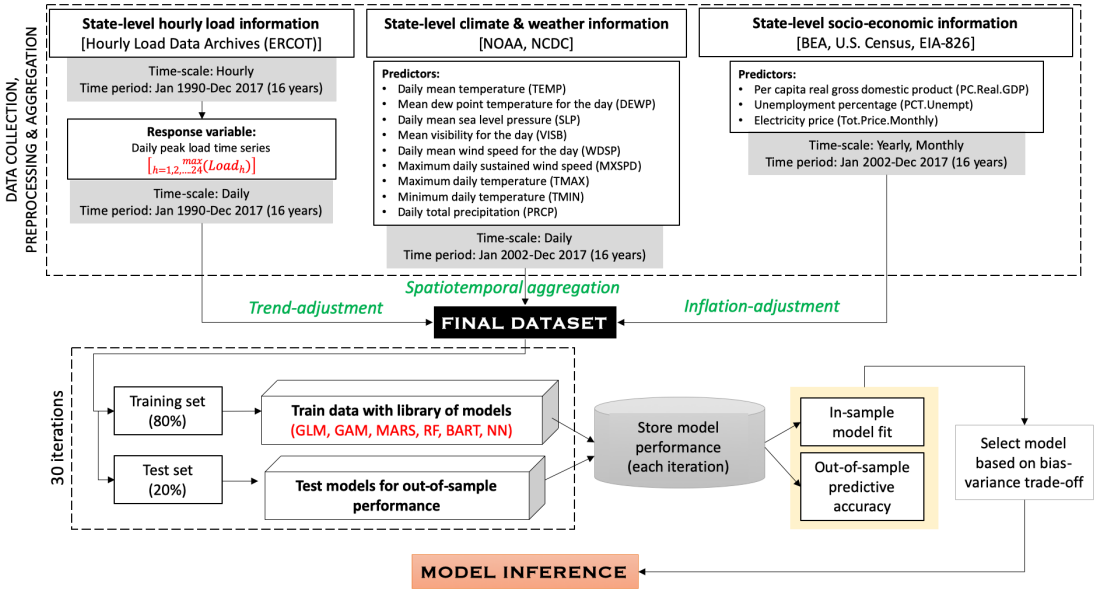

Figure 5: Research Framework

4.2. Statistical learning and model development

Supervised learning theory is leveraged to characterize the climate-daily peak load nexus. Broadly speaking, the goal of supervised learning is to estimate a function capable of predicting a statistical moment of a target variable (e.g., daily peak load) conditioned on one or more predictor variables (e.g, various climate variables), such that the loss function of interest (measuring the distance between the predictions and the observed values) is minimized. Supervised statistical learning methods can be parametric, semi-parametric or non-parametric. Parametric models generally assume a particular functional form that relates the

input variables to the response. The assumed functional forms help with ease of estimation and model interpretability, but come at the cost of predictive accuracy since the assumptions (such as normality and linearity) often do not hold for real data. Non-parametric models do not make many assumptions about the distribution of the response variable or the shape of the function relating the response to the predictors. Instead, they use the data in novel ways to approximate the dependencies. Their predictive power is generally superior to parametric models owing to their better approximation of the true functional forms. Moreover, non-parametric methods are data-intensive and highly dependent on data quality. In this research, the data is trained with a range of parametric and non-parametric supervised learning models to investigate the sensitivity of daily peak load to climate change. More specifically, the data is trained with generalized linear models (GLM), generalized additive models (GAM), multi-adaptive regression splines (MARS), and ensemble tree based models including random forest (RF), Bayesian additive regression trees (BART) and neural network (NN). While the overview of each of these algorithms is discussed in Appendix A, a brief explanation of the BART algorithm is provided in the following section since it was found to best capture the daily peak load–climate nexus.

4.2.1. Bayesian Additive Regression Trees (BART)

BART is a non-parametric, Bayesian, sum-of-trees model as shown in the equation below [34].

$$y = \sum_{i=1}^{m} g(x; T_j, M_j) + \epsilon; \quad where \quad \epsilon \sim N(0, \sigma^2) \tag{4}$$

$g(x; T, M)$ is the function which assigns the parameters of the terminal nodes

of trees to the predictors x. Regularization priors are used to control model's complexity and restrict the overwhelming influence of the large tree components. Regularization priors eliminate an individual tree's effect of being unduly influential on the sum-of-trees model [34].

4.2.2. Predictive accuracy vs. model interpretability

As mentioned earlier, flexible non-parametric methods generally have higher predictive power than the parametric models. The improved predictive power, however, comes at the cost of ease of interpretability. Partial dependence plots (PDPs) are efficient methods of conducting variable inference for non-parametric models. PDPs help in understanding the individual effects of the predictor variables (x_j) on the response variable in a ceteris paribus condition (i.e. controlling for all the other predictors). Mathematically, the estimated partial dependence function is given as [35]:

$$\widehat{f}(x_j) = \frac{1}{n}\sum_{i=1}^{n}\widehat{f}(x_j, x_{-j}, i) \tag{5}$$

Here, $\widehat{f}$ denotes the statistical model; n denotes the number of observations in the training dataset; x_{-j} denotes all the variables except x_j . The estimated PDP of the predictor x_j provides the average value of the function $\widehat{f}$ when x_j is fixed and x_{-j} varies over its marginal distribution.

4.2.3. Bias variance trade off

The generalization performance of a predictive model hinges on the ability to simultaneously minimize the bias and variance of the model. Cross validation is one of the most widely used methods for balancing bias and variance [30]. The method of k-fold cross validation is used to estimate predictive accuracy.

K-fold cross-validation involves randomly dividing the data into k equally-sized subsets. In each iteration, the model is fitted to all the data subsets except the k^{th} held-out subset, and the predictive accuracy is calculated based on the model's performance on the k^{th} held-out subset. In this paper, the out-of-sample model performance was estimated using a 20% holdout cross validation approach. The out-of-sample mean square error (MSE) and mean absolute error (MAE) are then calculated using the following formula [10]:

$$MSE_{out-of-sample} = \frac{1}{k}[\sum_{k=1}^{n}\frac{1}{m}(\sum_{i=1}^{m}(y_{i,k} - \widehat{y}_{i,k})^2)] \tag{6}$$

$$MAE_{out-of-sample} = \frac{1}{k}[\sum_{k=1}^{n}\frac{1}{m}|\sum_{i=1}^{m}(y_{i,k} - \widehat{y}_{i,k})|] \tag{7}$$

k= number of times cross validation is performed; m=number of holdouts during each cross validation $y_{i,k}$=ith actual observation that was randomly holdout during the k^{th} cross-validation $\widehat{y}_{i,k}$= predicted i^{th} observation during the k^{th} cross validation using the model developed using the training set data during the k^{th} cross validation

The model selection is conducted based on both in-sample fit and out-of-sample predictive accuracy. The in-sample error is measured using the in-sample MSE, MAE, and adjusted R^2 while the out-of-sample error was measured using the out-of-sample MSE and MAE as discussed above.

5. Results

Using each algorithm described in the methodology section, three sets of models are developed, namely, one using TMAX and DEWP (Model 1) [i.e.,

not including TEMP and TMIN], one using TEMP (Model 2) [i.e., excluding DEWP, TMAX, and TMIN], and finally a model using TMIN (Model 3) alone [i.e., excluding DEWP, TMAX, and TEMP], while keeping the non-temperature variables the same in all the models. The rationale for the development of three separate models are: 1) including highly correlated variables within the same model could mask the individual effects of the variables while inferencing; and 2) assessing separate models can help identify which temperature variable(s) best capture(s) the climate sensitivity of daily peak load. The results showed that the model with DEWP and TMAX outperformed the other two models. This is not surprising since (1) DEWP accounts for humidity which has been shown to be a key predictor of the electricity demand for space conditioning [10]; and (2) using TMAX can help capture temperature extremes in Texas which have occurred with a higher frequency in recent years leading to unanticipated demand surges during the hot spells [36].

5.1. Model Performance

Table 3 summarizes the goodness-of-fit and predictive performance of each of the trained models. The percentage improvement (%imp) metric is also provided in Table 4, indicating the percentage improvement yielded by each of the trained models over having no statistical model and using the historical average as a predictor (i.e., the 'mean-only' model) .

Table 3: Comparative assessment of the model performance.

#	Models	R^2	In-sample err.		Out-of-sample err.	
			RMSE	**MAE**	**RMSE**	**MAE**
1	Mean-only	-NA	-NA	-NA	9.399	8.202
2	GLM	0.526	6.499	5.375	6.494	5.363
3	GAM	0.874	3.337	2.626	3.379	2.660
4	MARS-1	0.861	3.518	2.761	3.530	2.772
5	MARS-2	0.880	3.264	2.542	3.274	2.545
6	MARS-3	0.886	3.186	2.487	3.239	2.515
7	MARS-4	0.886	3.186	2.487	3.240	2.516
8	RF	0.980	1.350	1.044	3.112	2.441
9	BART	0.930	2.500	1.928	2.866	2.213
10	NN	0.899	3.000	2.316	3.382	2.641

The predictive model is selected based on the BART algorithm as the final model, since it outperformed all the other models in terms of out-of-sample predictive accuracy (Tables 3-4). In terms of in-sample goodness of fit, the model based on the Random Forest algorithm ranked top, indicating potential overfitting of the data (Table 3).

To further examine the performance of the final best model (based on BART), the model predictions versus observed values of daily peak load (Figure 6) is plotted. The 95% credible intervals provide 56.09% coverage for all the observations (Figure 6a) whereas the 95% prediction interval offers a 97.09% coverage (Figure 6b).

The observed deviations at the tails of the Q−Q plot of the residuals (Figure

Table 4: Models' percentage improvement over the 'null' (i.e., mean-only) model.

Models	**Out-of-sample error (%imp)**	
	RMSE	**MAE**
GLM	31	35
GAM	64	68
MARS-1	62	66
MARS-2	65	69
MARS-3	66	69
MARS-4	65	69
RF	67	70
BART	***69***	***73***
NN	64	68

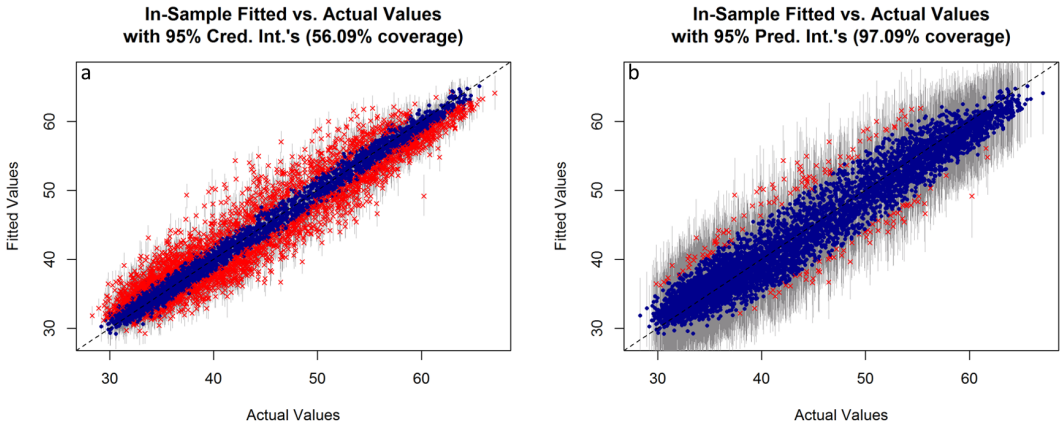

Figure 6: a. In-Sample fitted vs. actual values using 95% Credible Intervals. b. In-Sample fitted vs. actual values using 95% Prediction Intervals.

7) is attributable to other unobserved variables (probably non-climatic factors) that influence the daily peak load demand, but are not captured in the climate-

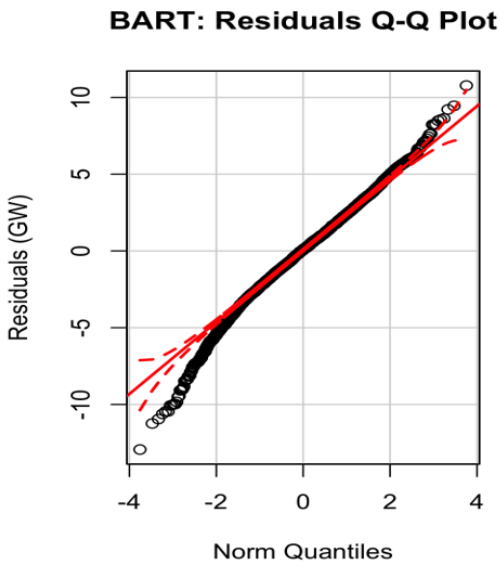

Figure 7: QQ-plot of the BART model (the red dashed lines in the QQ-plot represent 95% confidence intervals)

peak load nexus model presented in this paper.

5.2. Model Inference

The ranking of the important predictors influencing daily peak electricity load is given in Figure 8. The figure helps identify maximum temperature (TMAX) as the most important predictor followed by mean dew point temperature (DEWP), total monthly electricity price (Tot.Price.Monthly), and per capita real gross state product (PC.Real.GDP).

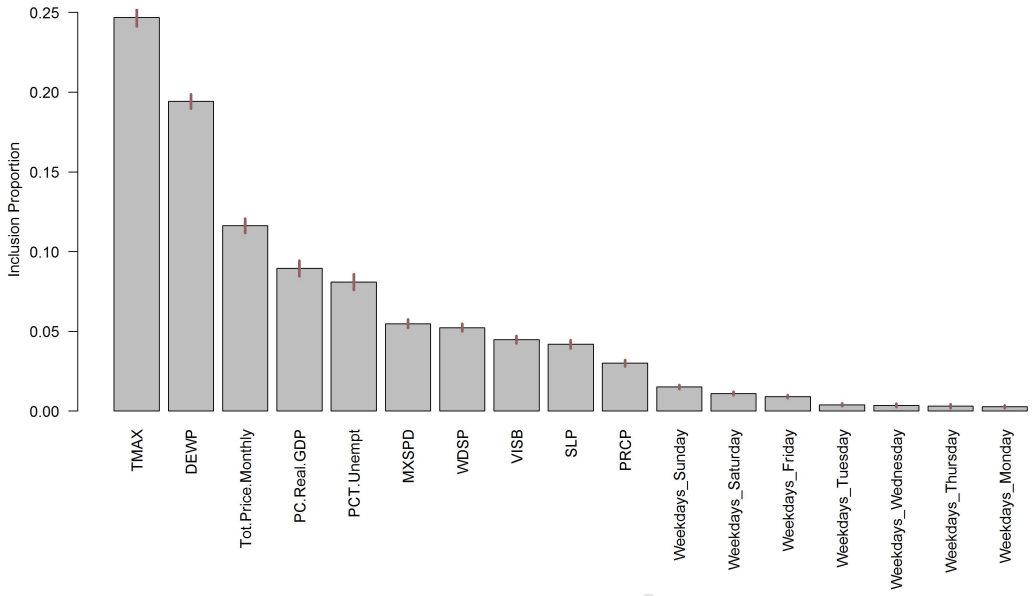

Figure 8: The ranking of the importance of the explanatory variables in contributing to the accuracy of the final best model.

The partial dependencies between the top six key predictors and daily peak load are plotted in the following sub-sections to characterize the marginal influence of the key predictors on the daily peak electricity demand.

5.2.1. Influence of maximum temperature and dew point temperature

The PDP of daily peak electricity load versus the maximum temperature (TMAX) (Figure 9a) shows an initial inverse relationship between load and increasing temperatures until 70°F/21°C and then an increasing trend thereafter. The marginal plot indicates that for a 30°F/-1°C increase in TMAX (70°F/21°C — 100°F/38°C), the daily peak load increases by 20 GW. Peak load is relatively insensitive to maximum temperature in the range of 67°F/19°C to 74°F/23°C since the need for space heating or cooling is minimum during temperate ranges.

The increasing trend associated with temperatures less than 67°F/19°C indicates increasing peak load due to increased space heating during colder winter days.

Figure 9b illustrates the PDP of daily peak electricity load versus the average daily dew point temperature. Three distinct regions are apparent in the figure. For days with colder dew point temperatures (i.e., colder and humid winter days with temperatures below 30°F/-1°C) the daily peak load increases as the dew point temperature decreases. This can be attributed to increased demand for space heating with decreasing temperatures. The peak load is minimum for DEWP in the range of 30°F/-1°C — 40°F/4°C and rapidly increases for warmer days (i.e. DEWP above 40°F/4°C)

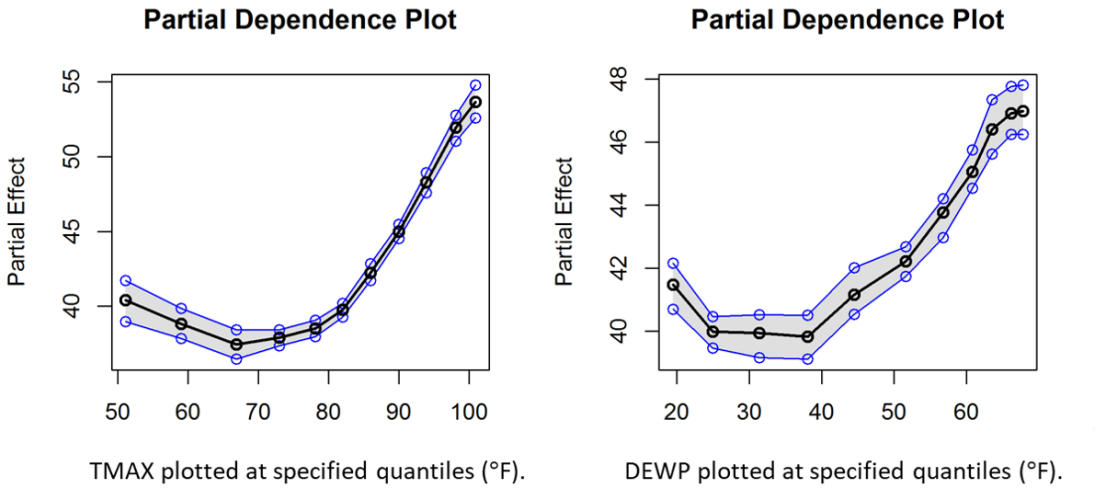

Figure 9: a. Influence of mean dew point temperature and b. Influence of maximum temperature on daily peak load.

5.2.2. Relationship with electricity price

Electricity price is found to be one of the most important non-climatic predictor of daily peak load. As discussed before, electricity price (along with other

socio-economic variables) is used as a 'control variable' to isolate the effect of climate on daily peak demand. However, since it is found to be among the key predictors of daily peak demand, a brief discussion of its relationship with the response variable is included. Figure 10 shows that the daily peak electricity load exhibit a positive correlation with the monthly mean electricity price which is in line with the existing literature [37] that indicates higher prices are charged during times of peak demands.

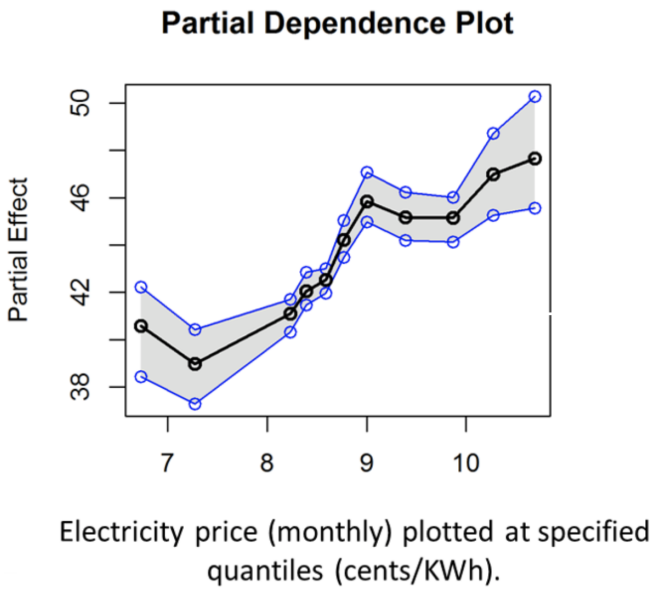

Figure 10: Influence of total monthly electricity price on daily peak load

5.2.3. Relationship with per capita gross state product

Figure 11 shows that the peak electricity load is decreasing with the economic growth in terms of per capita real gross domestic product (PC.Real.GDP). Economic growth is positively associated with socio-technical advancements such as more investments in new energy-efficient equipment. Moreover, with the signifi-

cant growth of cyber infrastructure and development of IOTs (internet of things), the key driver of economy has shifted away from heavy manufacturing industries to cyber business and service-oriented industry. A recent study by the American Council for an energy efficient economy argued that since the mid-1990s, much of the observed downward trend in the energy demand intensity associated with the economic growth can be attributed to the growth of such less energy-intensive cyber businesses [38].

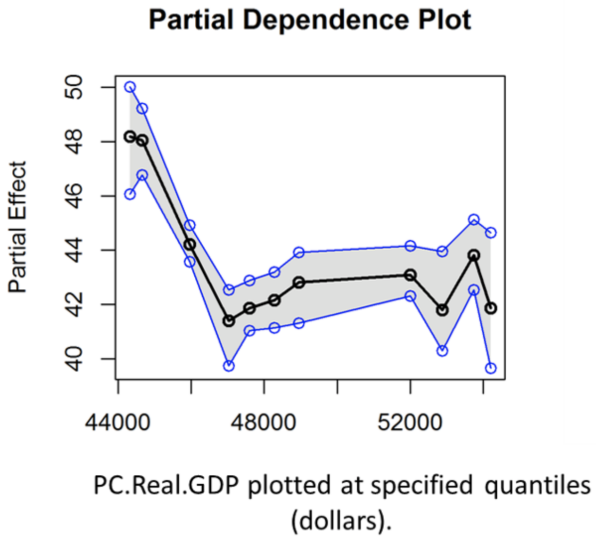

Figure 11: Influence of per capita gross state product on daily peak load.

5.2.4. Relationship of unemployment with peak load

The association of unemployment with the daily peak load (Figure 12) shows a random fluctuation. Although there is no significant upward or downward trend in the marginal peak load with increasing unemployment rates, the levels of uncertainty changes. The uncertainty bands (shaded gray area) are wider at

the higher percentage of unemployment, indicating a higher variability in peak loads associated with higher unemployment rates.

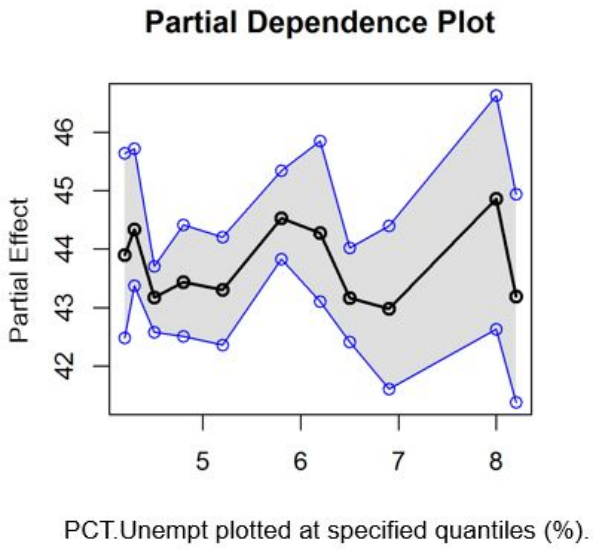

Figure 12: Influence of PCT.Unemployment (%) on daily peak load.

5.2.5. Influence of maximum sustained wind speed

Daily peak electricity load has an inverse relationship with increasing maximum sustained wind speeds (Figure 13). This is intuitive, as sustained winds lower the feels-like temperature, and increase the rate of evaporation from the human body as well as the built environment, and therefore, creating a cooling effect. Thus, during breezy/windy days the lower daily peak loads is attributable to lower electricity demands for space cooling [39].

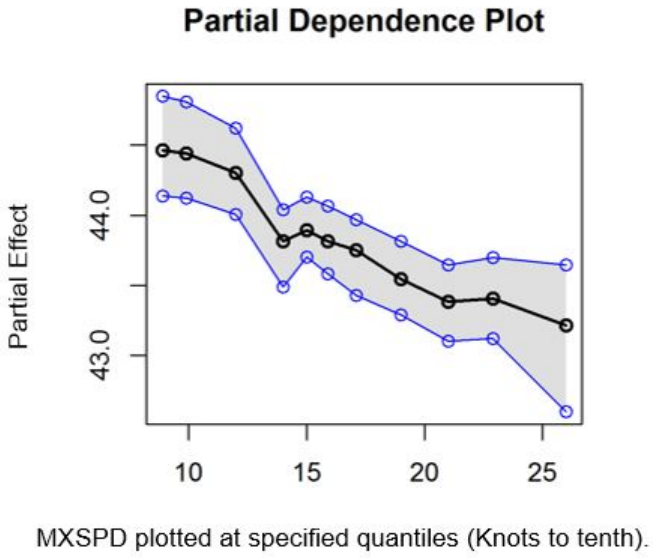

Figure 13: Influence of maximum sustained wind speed (Knots to tenth) reported for the day on daily peak load.

6. Conclusion

Effective adequacy planning in the electricity sector is requisite for achieving grid resilience, as it helps minimize significant supply surplus/shortages and thus mitigates unpredictable electricity price hikes and rolling blackouts, which often result in large-scale socio-economic losses. Effective adequacy planning hinges on access to accurate forecasts of demand patterns, particularly under exogenous shocks such as climate variability and change.

In this paper, the climate sensitivity of daily peak load is investigated using advanced machine learning algorithms. A generalized probabilsitic predictive framework is proposed—based on a Bayesian tree-ensemble algorithm—to assess the climate sensitivity of peak load and to identify its key predictors. Although the proposed model is used to characterize the climate sensitivity of the daily

peak load, it can also be leveraged for short-term (daily) peak load predictions as it outperforms all the other models in regards to explaining the variations in data as well as out-of-sample predictions.

The results revealed that maximum daily temperature followed by mean dew point temperature of a day are the most important predictors of the climate sensitive portion of the daily peak load in the state of Texas. Moreover, it is observed that when the maximum temperatures lie in the range of 67°F (19°C) — 74°F(23°C) and dew point temperatures in the range of 30°F(-1°C) — 40°F(4°C), the peak load is relatively temperature-insensitive. The results also indicated an inverse relationship between sustained wind speeds and daily peak load, with peak daily loads decreasing at higher sustained wind speeds. This inverse relationship is attributable to the cooling effect of the sustained winds.

Among the non-climatic predictors, the socio-economic variables such as electricity price, per capita gross domestic product, and percentage of unemployed populations were found to have a strong association with the daily peak load. The results indicated a strong positive association between the daily peak load and the electricity price, whereas the association between percent unemployed and the daily peak load was more uncertain. Economic growth was observed to have an inverse association with the peak load, mostly attributable to increased investments in energy efficient equipment as well as a move away from manufacturing-heavy industry to service/cyber industry.

The proposed framework in this study is transferable to other service areas, and can be used by utility planners and operators across the country to characterize the climate sensitivity of peak load. Moreover, the inferences from the Texas case study is of particular interest to the stakeholders in the ERCOT re-

gion that have faced frequent supply inadequacy risks during the more frequent episodes of heatwaves over the past decade. The study results demonstrate that the existing approaches based on parametric models (prevalent in many regions of the country including ERCOT) underperform in terms of predictive accuracy and thereby might underestimate the requisite reserve margins. Moreover, the existing approaches based on air temperature alone (that do not account for humidity levels) lead to understating the climate-sensitivity of peak load in the state, with big implications for grid resilience in the ERCOT region.

References

Bibliography

[1] Roshanak Nateghi. Multi-dimensional infrastructure resilience modeling: An application to hurricane-prone electric power distribution systems. *IEEE Access*, 6:13478–13489, 2018.

[2] Sayanti Mukherjee, Roshanak Nateghi, and Makarand Hastak. A multi-hazard approach to assess severe weather-induced major power outage risks in the us. *Reliability Engineering & System Safety*, 175:283–305, 2018.

[3] Sayanti Mukherjee and Roshanak Nateghi. A data-driven approach to assessing supply inadequacy risks due to climate-induced shifts in electricity demand. *Risk Analysis*, 39:673–694, 2019.

[4] Roshanak Nateghi, Seth D Guikema, Yue Wu, and C Bayan Bruss. Critical assessment of the foundations of power transmission and distribution reliability metrics and standards. *Risk analysis*, 36(1):4–15, 2016.

[5] Sayanti Mukhopadhyay and Roshanak Nateghi. Estimating climate-demand nexus to support longterm adequacy planning in the energy sector. pages 1–5, 2017.

[6] Leigh Raymond, Douglas Gotham, William McClain, Sayanti Mukherjee, Roshanak Nateghi, Paul V Preckel, Peter Schubert, Shweta Singh, and Elizabeth Wachs. Projected climate change impacts on indiana's energy demand and supply. *Climatic Change*, pages 1–15, 2018.

[7] Roshanak Nateghi and Sayanti Mukherjee. A multi-paradigm framework to assess the impacts of climate change on end-use energy demand. *PloS one*, 12:e0188033, 2017.

[8] Mustafa Lokhandwala and Roshanak Nateghi. Leveraging advanced predictive analytics to assess commercial cooling load in the us. *Sustainable Production and Consumption*, 14:66–81, 2018.

[9] Maximilian Auffhammer, Patrick Baylis, and Catherine H Hausman. Climate change is projected to have severe impacts on the frequency and intensity of peak electricity demand across the united states. *Proceedings of the National Academy of Sciences*, 114:1886–1891, 2017.

[10] Sayanti Mukherjee and Roshanak Nateghi. Climate sensitivity of end-use electricity consumption in the built environment: An application to the state of Florida, United States. *Energy*, 128:688–700, 2017.

[11] I Boustead and BR Yaros. Electricity supply industry in north america. *Resources, conservation and recycling*, 12:121–134, 1994.

[12] John Walewski, Jolanda P Prozzi, Steven Polunsky, et al. How vulnerable is texas freight infrastructure to extreme weather events? final report. Technical report, Texas A&M Transportation Institute, 2017.

[13] Chapter 4 climate of texas. `http://www.twdb.texas.gov/publications/state_water_plan/2012/04.pdf`.

[14] Texas - state energy profile analysis - u.s. energy information administration (eia). https://www.eia.gov/state/analysis.php?sid=TX, 2019. Last accessed 14 May 2019.

[15] Sayanti Mukherjee, CR Vineeth, and Roshanak Nateghi. Evaluating regional climate-electricity demand nexus: A composite bayesian predictive framework. *Applied Energy*, 235:1561–1582, 2019.

[16] Takeshi Haida and Shoichi Muto. Regression based peak load forecasting using a transformation technique. *IEEE Transactions on Power Systems*, 9:1788–1794, 1994.

[17] Takeshi Haida, Shoichi Muto, Yoshio Takahashi, and Yasutaka Ishi. Peak load forecasting using multiple-year data with trend data processing techniques. *Electrical Engineering in Japan*, 124:7–16, 1998.

[18] Ramu Ramanathan, Robert Engle, Clive W.J. Granger, Farshid Vahid-Araghi, and Casey Brace. Short-run forecasts of electricity loads and peaks. *International Journal of Forecasting*, 13:161–174, 6 1997.

[19] HK Alfares and M Nazeeruddin. Regression-based methodology for daily peak load forecasting. 3:468–471, 1999.

[20] A.D. Papalexopoulos and T.C. Hesterberg. A regression-based approach to short-term system load forecasting. *IEEE Transactions on Power Systems*, 5:1535–1547, 1990.

[21] N. Amjady. Short-term hourly load forecasting using time-series modeling with peak load estimation capability. *IEEE Transactions on Power Systems*, 16:798–805, 2001.

[22] Cheng Fan, Fu Xiao, and Shengwei Wang. Development of prediction models for next-day building energy consumption and peak power demand using data mining techniques. *Applied Energy*, 127:1–10, 2014.

[23] Caston Sigauke and Delson Chikobvu. Daily peak electricity load forecasting in south africa using a multivariate non-parametric regression approach. *ORiON*, 26:97–111, 2010.

[24] Jun M Liu, Rong Chen, Lon-Mu Liu, and John L Harris. A semi-parametric time series approach in modeling hourly electricity loads. *Journal of Forecasting*, 25:537–559, 2006.

[25] Peter Lusis, Kaveh Rajab Khalilpour, Lachlan Andrew, and Ariel Liebman. Short-term residential load forecasting: Impact of calendar effects and forecast granularity. *Applied Energy*, 205:654–669, 2017.

[26] Yibo Chen, Hongwei Tan, and Xiaodong Song. Day-ahead forecasting of non-stationary electric power demand in commercial buildings: Hybrid support vector regression based. *Energy Procedia*, 105:2101–2106, 2017.

[27] Mohanad S Al-Musaylh, Ravinesh C Deo, Jan F Adamowski, and Yan Li.

Short-term electricity demand forecasting with mars, svr and arima models using aggregated demand data in queensland, australia. *Advanced Engineering Informatics*, 35:1–16, 2018.

[28] M Beccali, M Cellura, V Lo Brano, and A Marvuglia. Short-term prediction of household electricity consumption: Assessing weather sensitivity in a mediterranean area. *Renewable and Sustainable Energy Reviews*, 12:2040–2065, 2008.

[29] LM Saini and MK Soni. Artificial neural network based peak load forecasting using levenberg–marquardt and quasi-newton methods. *IEE Proceedings-Generation, Transmission and Distribution*, 149:578–584, 2002.

[30] Jerome Friedman, Trevor Hastie, and Robert Tibshirani. *The elements of statistical learning*, volume 1. Springer series in statistics New York, 2001.

[31] American community survey (acs). https://www.census.gov/programs-surveys/acs/.

[32] Historical information on hourly loads by ercot for the years 1995-2018. `http://www.ercot.com/gridinfo/load/load_hist/`, 2009 (accessed April 1, 2018).

[33] David J Sailor and J Ricardo Muñoz. Sensitivity of electricity and natural gas consumption to climate in the usa—methodology and results for eight states. *Energy*, 22:987–998, 1997.

[34] Hugh A Chipman, Edward I George, and Robert E Mcculloch. BART:

BAYESIAN ADDITIVE REGRESSION TREES 1,2. *The Annals of Applied Statistics*, 4:266–298, 2010.

[35] Adam Kapelner and Justin Bleich. bartMachine: Machine Learning with Bayesian Additive Regression Trees. *arXiv preprint arXiv:1312.2171*, 2013.

[36] Mel Gabriel and Jatin Nathwani. Meeting the texas electricity peak demand conundrum: A case for wind and solar. *The Electricity Journal*, 31:57–64, 2018.

[37] Jacopo Torriti. Price-based demand side management: Assessing the impacts of time-of-use tariffs on residential electricity demand and peak shifting in northern italy. *Energy*, 44:576–583, 2012.

[38] John A Laitner and Karen Ehrhardt-Martinez. Information and communication technologies: The power of productivity (part ii). *Environmental Quality Management*, 18:19–35, 2009.

[39] Muhammad Usman Fahad and Naeem Arbab. Factor affecting short term load forecasting. *Journal of Clean Energy Technologies*, 2:305–309, 2014.

[40] J A Nelder and R W M Wedderburn. Generalized Linear Models. *Source Journal of the Royal Statistical Society. Series A (General) J. R. Statist. Soc. A*, 135:370–384, 1972.

[41] Jerome H Friedman. Multivariate Adaptive Regression Splines. *Source: The Annals of Statistics The Annals of Statistics*, 19:1–67, 1991.

[42] Warren S McCulloch and Walter Pitts. A logical calculus of the ideas imma-

nent in nervous activity. *The bulletin of mathematical biophysics*, 5:115–133, 1943.

Nomenclature:

BART Bayesian Additive Regression Trees

DEWP Mean Dew Point for the Day

GAM Generalized Additive Model

GLM Generalized Linear Model

GDP Gross Domestic Product (millions of USD measured in 2009 real dollars)

GW Gigawatt-hour

MAE Mean Absolute Error

MARS Multi Adaptive Regression Spline

MXSPD Maximum Sustained Wind Speed for the Day

NN Neural Network

PRCP Total Daily Precipitation

RF Random Forest

RMSE Root Mean Squared Error

SLP Mean Sea Level Pressure for the Day

TEMP Mean Temperature for the Day

TMIN Minimum Daily Temperature

TMAX Maximum Daily Temperature

VISB Mean Visibility for the Day

WDSP Mean Wind Speed for the Day

Appendix A.

Appendix A.1. Methodology Description

Appendix A.1.1. Generalized Linear Model

Generalized linear models (GLMs) extend linear regression, by relaxing the normality assumption; allowing the response to be generated from the exponential family distribution and be related to the predictors through a link function [40]. A generalized linear model is characterized by:

A dependent variable Y whose distribution is of the class of normal, binomial and Poisson or gamma or Inverse-Gaussian as shown in the equations below:

$$y_i \sim f_{y_i}$$
$$F_{y_i}(y_i) = exp\frac{y_i\theta_i - b(\theta_i)}{a(\phi)} + c(y_i, \phi) \tag{A.1}$$

That θ and ϕ are the location and scale parameters respectively.

A set of independent variables x_i.

A link function g(.) tying the parameters of the response to the linear combination of the input variables.

Appendix A.1.2. Generalized Additive Model

A Generalized Additive Model (GAM) is considered a semi-parametric technique. It relaxes the linearity assumption of generalized linear model, allowing for local non-linarites. The model assumes that response y has a distribution with the mean μ=$[E|x_1, x_2, ...x_p]$. Where each f_j is a smoothing function of a specified class of functions estimated non-parametrically, like regression splines and tensor product splines. Multivariate Adaptive Regression Splines

$$g(\mu_i) = \alpha + \sum_{j=1}^{p} f_i(x_i) \tag{A.2}$$

Appendix A.1.3. Multivariate Adaptive Regression Splines

Multivariate Adaptive Regression Splines (MARS) is semi-parametric, adaptive procedure for regression, well suited for high dimensional problems [41]. It can be viewed as a generalization of stepwise linear regression. A MARS model consists of sum-of-splines that allow the response to vary non-linearly with the

input variables as shown in the equation below.

$$f(x) = \beta_0 + \sum_{m=1}^{M} B_m h_m(x) \tag{A.3}$$

Where each h_m(x) represents the linear splines, β_0 represents the intercept and β_m represents the vector of the coefficients. m coefficients are estimated by minimizing the sum of square errors.

Appendix A.1.4. Random Forest

Random Forest (RF) is a non-parametric, tree-based ensemble data-miner [**?**]. The method consists of B bootstrapped regression trees (T_b); with B selected based on cross-validation. Regression trees are low-bias high variance techniques. In other words, they can capture the structure of the data really well (low bias), but are highly sensitive to outliers (high variance). RF leverages model averaging as a variance reduction technique. The final estimate is therefore, the average of predictions across all trees as shown in the equation below.

$$\widehat{f}_{rf}^{B}(x) = \frac{1}{B} \sum_{b=1}^{B} T_b(x) \tag{A.4}$$

Appendix A.1.5. Neural network

Artificial Neural Networks (ANNs) are inspired by the biological nervous system to model the learning behavior of human brain and is a non-parametric model. The first artificial neuron was produced in 1943 by the neurophysiologist Warren McCulloch and the logicial Walter Pits [42]. A single neuron in a multilayer neural network. The various weighted inputs are fed into the single neuron. There are two functions that come into play inside a neuron; namely, Transfer function and Activation function.

The transfer function (or we could call it the aggregator) sums up all these weighted inputs. Let us denote the transfer function as z given as

$$z = \sum_{x=1}^{n} w_i x_i + w_b b \tag{A.5}$$

The activation function (or the squash function) squashes the output value of the transfer function into a defined range. It is used define the rate of firing from the neuron. Activation functions could be linear and non-linear. A straightforward activation function could be $f(z) = z$ which preserves the input as it is. However the limits are not defined in this function. In order to better denote the rate of firing, the activation function commonly used in the sigmoid function. The type of the neuron is defined from its activation function as well. Neurons with sigmoid activation functions are called sigmoid neurons. Let us denote the activation function as α and the sigmoid activation function is given as:

$$\alpha = \sigma(Z) = \frac{1}{1 + e^{-z}} \tag{A.6}$$

The sigmoid function has the property of differentiability throughout and a defined boundary in both the extremes. Another reason why we chose sigmoid is because of having a mathematical convenience. Let us see why that is by differentiating the sigmoid function:

$$\sigma' = \frac{d}{dz} \frac{1}{(1 + e^{-z})} \tag{A.7}$$

$$= \frac{1}{(1 + e^{-z})} \frac{d}{dz} (e^{-z}) \tag{A.8}$$

$$= \frac{e^{-z}}{(1 + e^{-z})} \frac{1}{(1 + e^{-z})} \tag{A.9}$$

$$= \frac{e^{-z}+1-1}{(1+e^{-z})}\frac{1}{(1+e^{-z})} \tag{A.10}$$

$$= (\frac{(1+e^{-z})}{(1+e^{-z})} - \frac{1}{(1+e^{-z})})\frac{1}{(1+e^{-z})} \tag{A.11}$$

Appendix A.2. Results

In this section, the results of the models − Model 2 (using TEMP as the only temperature variable and excluding DEWP, TMAX, TMIN) and Model 3 (using TMIN as the only temperature variable and excluding DEWP, TMAX, TEMP) − that we have not explained in the main text of the paper are presented.

Appendix A.2.1. Model 1

Table A.5: Comparative assessment of the models' in-sample and out-of-sample predictive performances (Model 1).

#	Models	Tuning parameters	R^2	In-sample err.		Out-of-sample err.	
				RMSE	MAE	RMSE	MAE
1	Mean-only	-NA	-NA	-NA	-NA	9.399	8.202
2	GLM	k=2.0, Both, Dist.=Gaussian	0.526	6.499	5.375	6.494	5.363
3	GAM	Stepwise update	0.874	3.337	2.626	3.379	2.660
4	MARS-1	pMethod: backward; nfold: 10; ncross=5	0.861	3.518	2.761	3.530	2.772
5	MARS-2	pMethod: cv; nfold: 10; ncross=5; degree=2	0.880	3.264	2.542	3.274	2.545
6	MARS-3	pMethod: cv; nfold: 10; ncross=5; degree=3	0.886	3.186	2.487	3.239	2.515
7	MARS-4	pMethod: backward; nfold: 10; ncross=5; degree=3, penalty 2	0.886	3.186	2.487	3.240	2.516
8	RF	mtry=p/3 =4; ntree=3867	0.980	1.350	1.044	3.112	2.441
9	BART	k=2,nu=3,q=0.99,m=200	0.930	2.500	1.928	2.866	2.213
10	NN	Hidden units (size)=9; Weight decay (Decay)=0.001	0.899	3.000	2.316	3.382	2.641

Model 1 is explained in details in the main body of the paper. However, we have included this table in the Appendix again to indicate the tuning parameters

of the models that we leveraged to explain the climate−peak load nexus.

Appendix A.2.2. Model 2

Table A.6: Comparative assessment of the models' in-sample and out-of-sample predictive performances (Model 2).

#	Models	Tuning parameters	R^2	In-sample err.		Out-of-sample err.	
				RMSE	MAE	RMSE	MAE
1	Mean-only	-NA	-NA	-NA	-NA	9.462	8.258
2	GLM	k=2.0, Both, Dist.=Gaussian	0.566	6.221	5.106	6.187	5.094
3	GAM	Stepwise update	0.900	2.963	2.329	2.996	2.355
4	MARS-1	pMethod: backward; nfold: 10; ncross=5	0.890	3.134	2.445	3.143	2.459
5	MARS-2	pMethod: cv; nfold: 10; ncross=5; degree=2	0.905	2.916	2.265	2.937	2.285
6	MARS-3	pMethod: cv; nfold: 10; ncross=5; degree=3	0.906	2.889	2.236	2.910	2.263
7	MARS-4	pMethod: backward; nfold: 10; ncross=5; degree=3, penalty 2	0.906	2.889	2.236	2.910	2.263
8	RF	mtry=p/3 =3; ntree=3831	0.981	1.297	1.012	2.916	2.300
9	BART	k=2,nu=3,q=0.9,m=200	0.938	2.345	1.798	2.609	2.010
10	NN	Hidden units (size)=9; Weight decay (Decay)=0.001	0.910	2.831	2.187	2.886	2.233

From the above Table A.6 it is again observed that the BART model outperformed all the other models in terms of out-of-sample predictive accuracy, and ranks second in terms of in-sample goodness of fit (after RF model). Thus, BART was determined to be the final model in this case as well. The variable importance plots (Figure A.14), residuals Q−Q plot (Figure A.15), credible and prediction interval plots (Figure A.16), and the partial dependence plots of the top six important predictors (Figure A.17) (as identified from the variable importance plot) are included in this subsection.

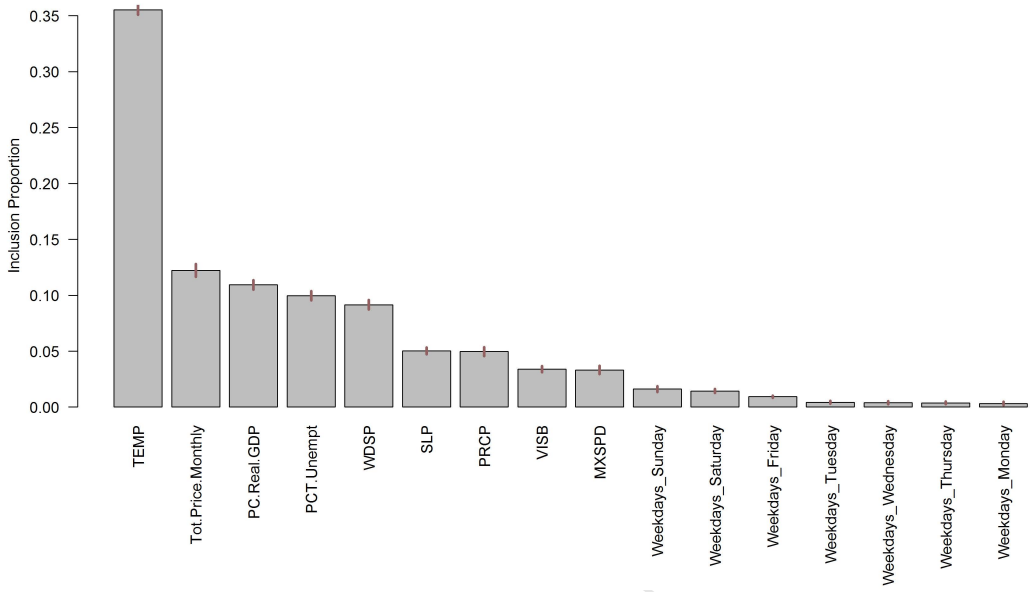

Figure A.14: Importance of each of the explanatory variables used in the BART model for predicting daily peak load (Model 2).

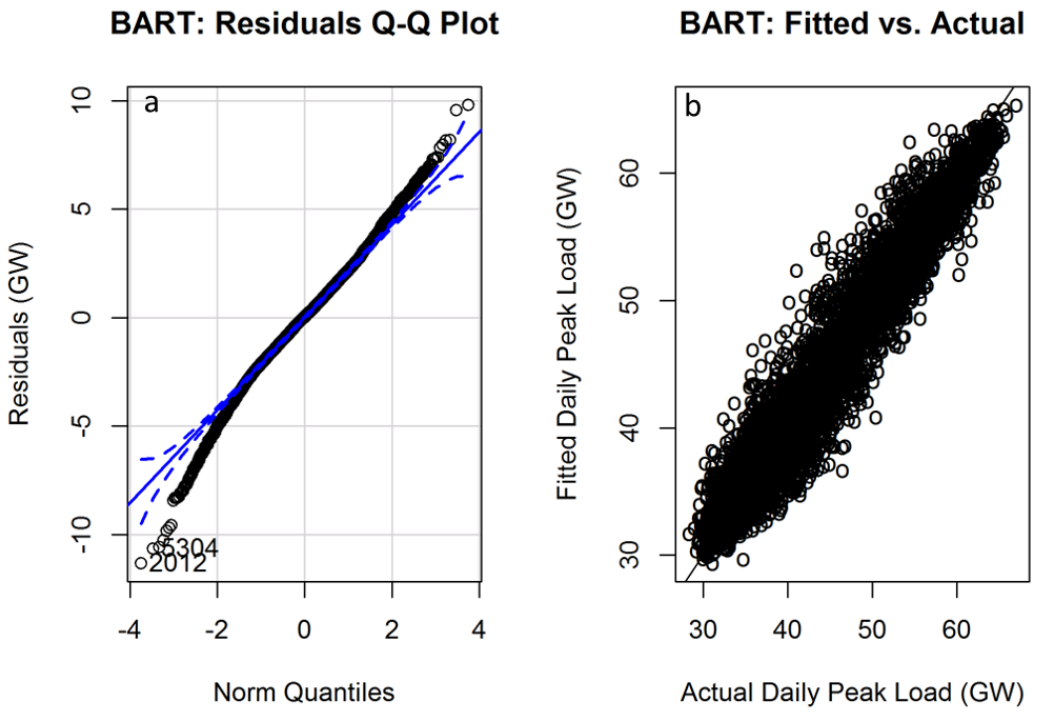

Figure A.15: a. Residual plots of the fitted BART models. b. Plot of observed versus fitted values of daily peak load for methods of BART (Model 2). The blue dashed lines in the QQ-plot represent 95% confidence intervals.

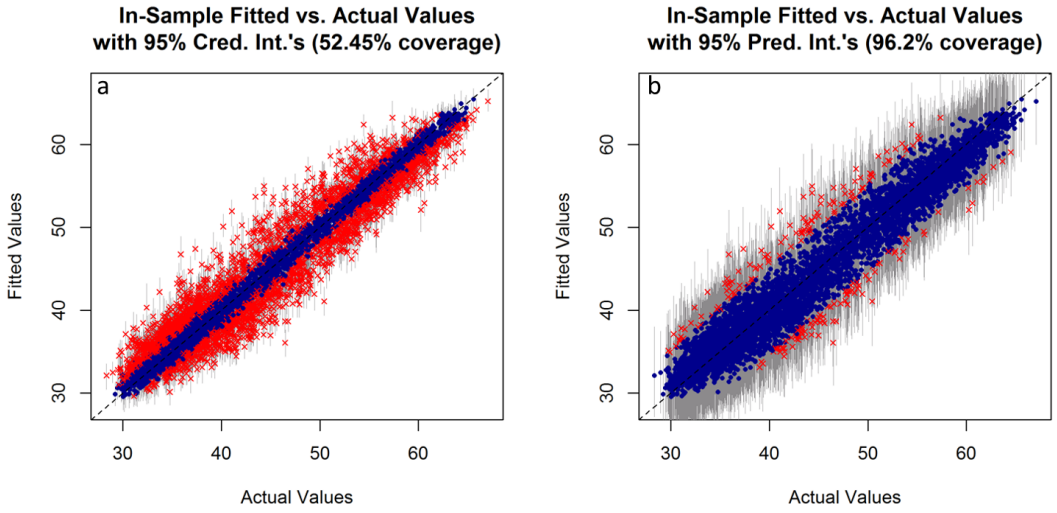

Figure A.16: a. In-Sample fitted vs. actual values using 95% Credible Intervals. b. In-Sample fitted vs. actual values using 95% Prediction Intervals (Model 2).

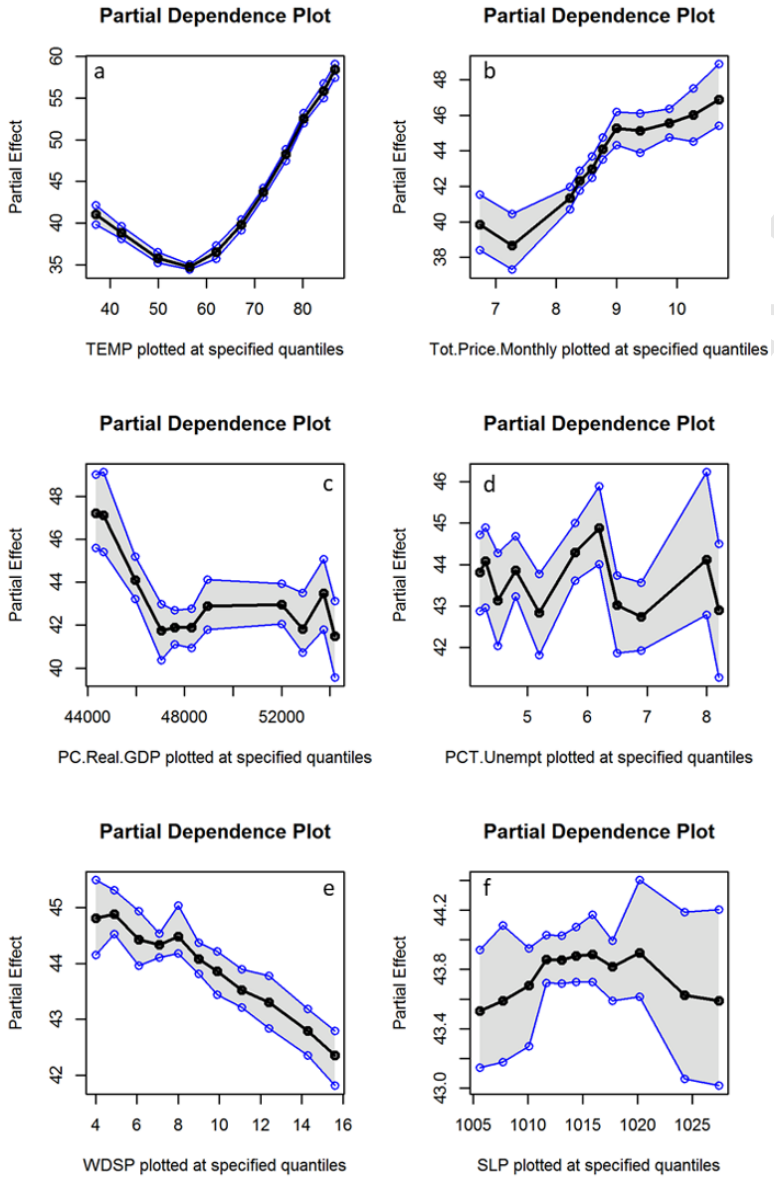

Figure A.17: Partial dependencies of the top six key predictors of (a) Mean daily temperature (in °F), (b) total monthly electricity price, (c) per capita real gross state product, (d) percentage of unemployment, (e) Mean wind speed for the day (in knots to tenths) and (f) Mean sea level pressure for the day (in Millibars to tenths), for the Model 2.

Appendix A.2.3. Model 3

Table A.7: Comparative assessment of the models' in-sample and out-of-sample predictive performances (Model 3).

#	Models	Tuning parameters	R^2	In-sample err.		Out-of-sample err.	
				RMSE	MAE	RMSE	MAE
1	Mean-only	-NA	-NA	-NA	-NA	9.455	8.252
2	GLM	k=2.0, Both, Dist.=Gaussian	0.565	6.228	5.152	6.270	5.175
3	GAM	Stepwise update	0.836	3.804	2.989	3.858	3.029
4	MARS-1	pMethod: backward; nfold: 10; ncross=5	0.828	3.915	3.064	3.981	3.112
5	MARS-2	pMethod: cv; nfold: 10; ncross=5; degree=2	0.844	3.733	2.889	2.925	2.925
6	MARS-3	pMethod: cv; nfold: 10; ncross=5; degree=3	0.843	3.737	2.898	3.785	2.924
7	MARS-4	pMethod: backward; nfold: 10; ncross=5; degree=3, penalty 2	0.843	3.737	2.898	3.785	2.924
8	RF	mtry=p/3 =3; ntree=3879	0.971	1.613	1.253	3.594	2.812
9	BART	k=2,nu=10,q=0.75,m=200	0.905	2.904	2.256	3.274	2.538
10	NN	Hidden units (size)=9; Weight decay (Decay)=0.001	0.856	3.586	2.761	3.701	2.851

From the above Table A.7 it is observed that the BART model outperformed all the other models in terms of out-of-sample predictive accuracy, and ranks second in terms of in-sample goodness of fit (after the RF model). Thus, similar to Model 1 and Model 2, BART was determined to be the final model in this case as well. The variable importance plots (Figure A.18), residuals Q−Q plots (Figure A.19), credible and prediction interval plots (Figure A.20), and the partial dependence plots of the top six important predictors (Figure A.21) (as identified from the variable importance plot) are included in this subsection.

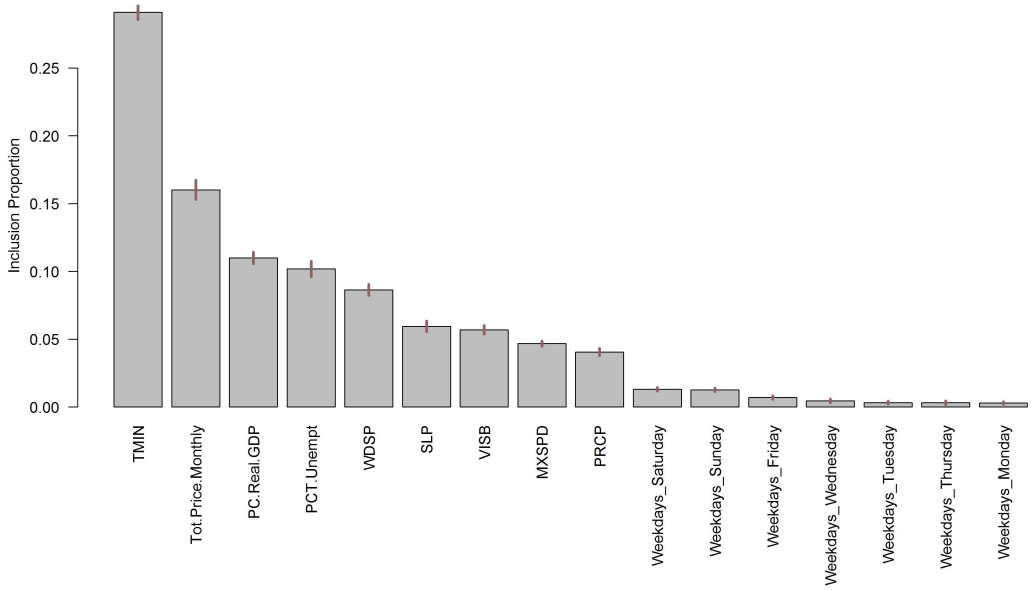

Figure A.18: Importance of each of the explanatory variables used in the BART model for predicting daily peak load (Model 3).

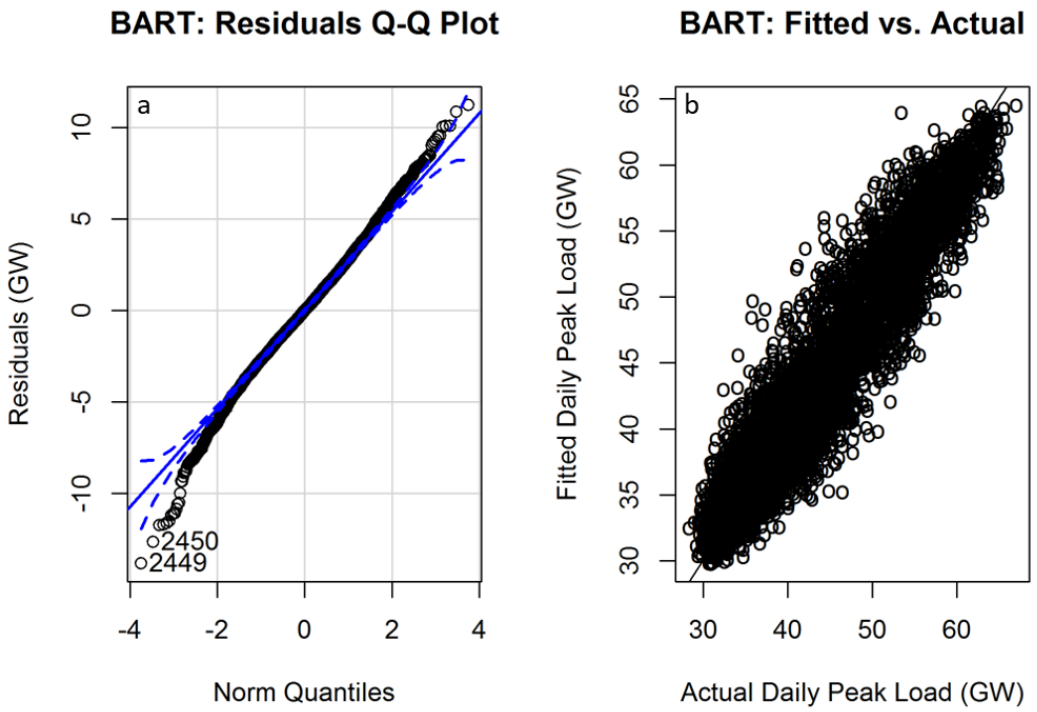

Figure A.19: a. Residual plots of the fitted BART models. b. Plot of observed versus fitted values of daily peak load for methods of BART. The blue dashed lines in the QQ-plot represent 95% confidence intervals. (Model 3).

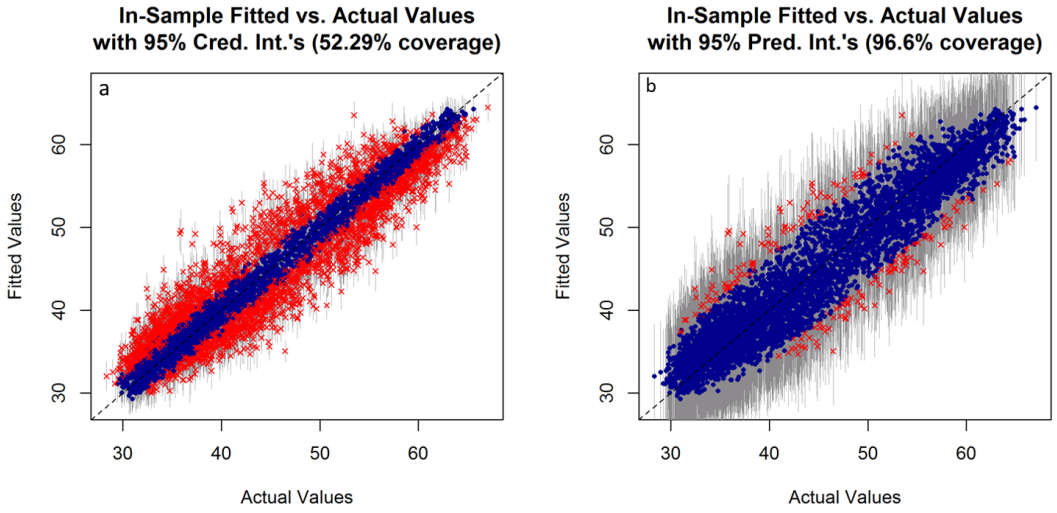

Figure A.20: a. In-Sample fitted vs. actual values using 95% Credible Intervals. b. In-Sample fitted vs. actual values using 95% Prediction Intervals (Model 3).

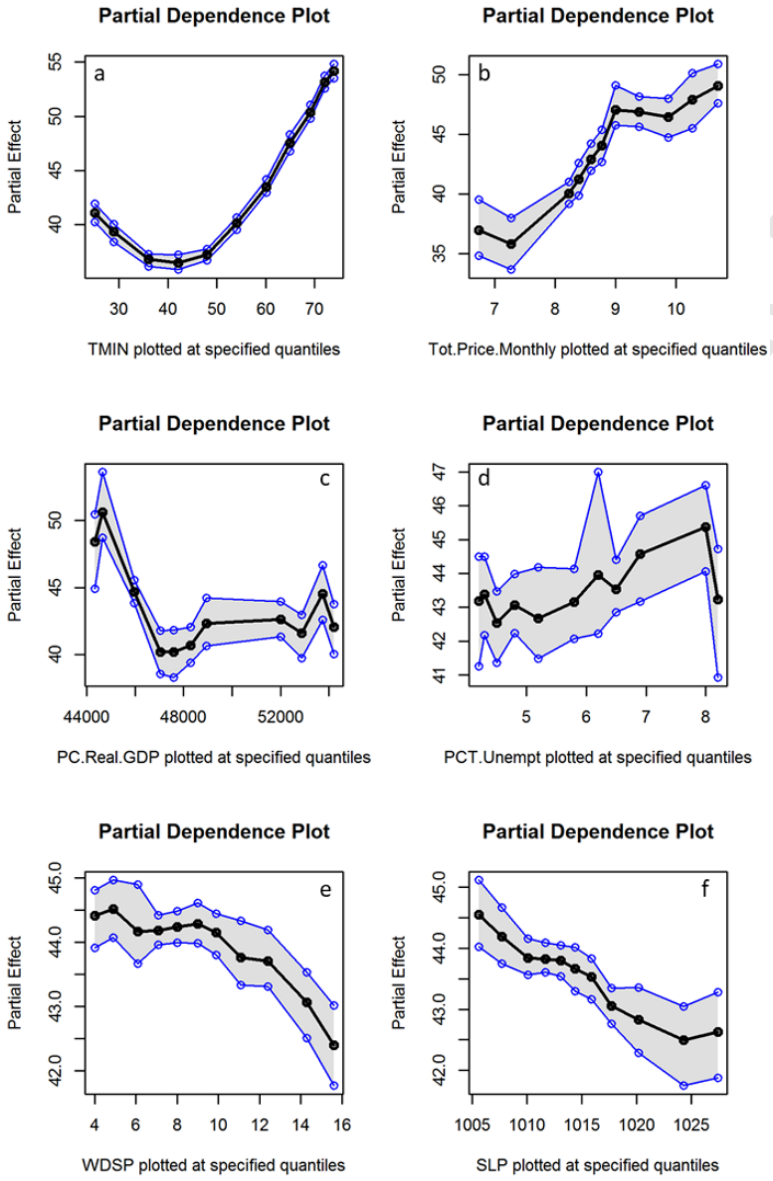

Figure A.21: Partial dependencies of the top six key predictors of (a) Minimum daily temperature (in °F), (b) total monthly electricity price, (c) per capita real gross state product, (d) percentage of unemployment, (e) Mean wind speed for the day (in knots to tenths) and (f) Mean sea level pressure for the day (in Millibars to tenths), for the Model 3.

Conflict of Interest Statement

There is no conflict of interest for this research.